

# Optimizing Crystal Size Distribution Based on Different Cooling Strategies in Batch Crystallization Process

Siti Zubaidah Adnan \*

Noor Asma Fazli Abdul Samad \*

Faculty of Chemical & Process Engineering Technology, Universiti Malaysia Pahang Al-Sultan Abdullah, Lebuhr Persiaran Tun Khalil Yaakob, 26300 Kuantan, Pahang, Malaysia

\*e-mail: siti.eiju@gmail.com (S.Z.A.); asmafazli@ump.edu.my (N.A.F.A.S)

*Submitted* 13 February 2024

*Revised* 20 November 2024

*Accepted* 6 December 2024

---

**Abstract.** Crystal size distribution (CSD) is an essential criterion for determining the production of high-quality crystals since it influences the efficiency of the crystallization process. Producing specified CSD in the crystallization process represents a main challenge as it depends on temperature control, which indirectly regulates the solution's concentration and affects the crystal's evolution. Different temperature profiles may influence the distribution of crystal products, and a suitable optimization algorithm is required to produce an optimum temperature trajectory that produces the desired CSD. Thus, this study aims to maximize the CSD of the grown seed crystals while minimizing the nucleus-grown crystals by employing the best optimization algorithm for the potash alum crystallization process. The crystallization process was developed and simulated in Matlab software using a potash alum in the water system. Four optimization algorithms were proposed with different objective functions, such as maximizing mean crystal size (I), minimizing coefficient of variation (II), minimizing nucleus-grown crystals (III), and maximizing CSD (IV). Based on the simulation results, optimization IV, which maximizes CSD, performs best with a large mean crystal size of 490  $\mu\text{m}$ . Furthermore, the number of fine crystals was among the lowest at a volume distribution of 0.00071  $\text{m}^3/\text{m}$  compared to the linear profile at 0.00191  $\text{m}^3/\text{m}$ . Optimization IV employs a dissolution strategy, which manipulates two quality specifications in one algorithm (size of crystals and number of fines), which is considered the best optimal cooling profile for seeded batch crystallization by maximizing CSD and minimizing the generation of nucleus-grown crystals.

**Keywords:** Cooling Profiles, Crystallization, Crystal Size Distribution, Dissolution, Optimization Algorithm, Temperature Control

## INTRODUCTION

In a batch-cooling crystallization process, the quality of crystal products ensures the efficient production of crystals (Walla *et al.*, 2023). Efficient production ensures smooth operation in the downstream processes such as filtering, washing, drying, storing, and transporting the crystals. One of the critical

product specifications that should be met to achieve process efficiency is crystal size distribution (CSD). CSD is a crucial product specification that directly affects the operation during downstream processes (Adnan and Samad, 2022; Zong *et al.*, 2023). Achieving an acceptable CSD range, such as a larger mean size with a reduced number of fine crystals, is recommended to avoid further

---

difficulties in the latter processing line and decrease process efficiency. For example, large-size crystals with a minimum number of fines are easy to separate for further processing during the filtration process. In contrast, small-sized crystals with fines will add more complexity and additional time to the crystal purification process. Therefore, it is essential to be attentive to the quality specifications of the crystals to ensure the required standards are met (Zheng *et al.*, 2022).

Generally, CSD is achieved by controlling the temperature of the solution. This indirectly regulates the concentration, which means supersaturation-dependent phenomena such as nucleation and crystal growth are altered, too. This action contributes to crystal properties such as purity, morphology, and CSD (Lee *et al.*, 2019; Samad *et al.*, 2010). Thus, selecting a proper temperature profile that can achieve the desired crystal product is important. Conventional cooling temperature profiles, which are linear and cubic cooling curves, are widely used for crystallization (Zhang *et al.*, 2018). This is because the linear cooling profile, for example, is expected to produce grown seed crystals whose CSD is superior to the natural cooling profile but a bit inferior to the cubic cooling curve. However, both cooling curves will generate many fine crystals at the end of the crystallization process (Hojjati and Rohani, 2005; Zhang *et al.*, 2018). These fine crystals are not desirable in the crystallization process as obtaining significant fine crystals may cause yield loss (Agrawal and Paterson, 2015) and long operational time, especially in filtration and drying processes (Trampuž *et al.*, 2021). Alternatively, to avoid these issues and thus achieve a better CSD profile with fewer fine crystals, an optimization algorithm may help

reduce the number of fine crystals. An optimization algorithm that comprises a specific control objective could be utilized for a given crystallization system.

Furthermore, an optimization algorithm was used decades ago to achieve optimal cooling policy regarding specified production targets related to CSD (Nagy *et al.*, 2019). The objective function can be set to maximize crystal size with subjected optimization limits or constraints such as total batch time, seed loading ratio, and temperature. The commonly used objective functions related to CSD available in the literature are the maximization of mean crystal size (Sanzida and Nagy, 2019), minimization of coefficients of variation (CV) (Ashraf and Rao, 2022; Hemalatha *et al.*, 2018), minimization of nucleus-grown crystals (fine crystals) (Ashraf and Rao, 2022; Seki and Su, 2015) and maximization of CSD (Nagy *et al.*, 2019; Trampuž *et al.*, 2021). However, no versatile optimization algorithm warrants suitability for all crystallization systems. Each optimization algorithm may only produce an optimal cooling profile for achieving the pre-set objective function in the given crystallization system and may not be effective in other systems. Several algorithms may need to be performed to evaluate the suitability and performance of the output to apply any chosen optimization algorithm to a new crystallization system. The underlying principles used in the first three common optimization algorithms are increasing crystal size (maximization of mean crystal size), improving the radical of crystals in each area against particle size (minimization of CV), and enhancing its nucleated-to-seed ratio (minimization of fine crystals), respectively. These optimizations are all a direct computation to achieve preferred characteristics of the crystalline products at

---

the end of the batch process. For the last common optimization algorithm (maximization of CSD), the dissolution strategy, which, on the other hand, manipulates the ramping of temperature as a distribution shaping tool to achieve the desired quality for an optimal crystallization system. No direct computation is used in this algorithm; instead, manipulation of the crystallization mechanism (dissolution). Moreover, dissolution strategy is the recent interest in the literature where it can be used to thwart the impacts of secondary nucleation that reduce the efficiency of the process by in situ fines removal (Nagy *et al.*, 2019; Szilágyi, 2022). The proposed optimal temperature profile, capable of obtaining large-sized crystals and reduced fine crystals for seeded batch crystallization via potash alum as a studied material, is the novelty of this paper.

Therefore, this paper aims to implement an optimal temperature profile using a dissolution optimization algorithm by maximizing the CSD of the grown seed crystals and minimizing the nucleus-grown crystals for the potash alum crystallization process. Matlab software develops the mathematical model for the seeded batch crystallization process. The simulation of the crystallization process using potash alum in the water system is adapted from (Aamir, 2010) and is selected arbitrarily for illustration purposes. Then, three other optimization algorithms with the objective function of maximizing mean crystal size, minimizing CV, and minimizing nucleus-grown crystals are employed against the dissolution algorithm. These optimizations are chosen to provide a variety of cooling profiles for potash alum adapted from the commonly used optimization algorithms in literature for analysis purposes. The performance of each

generated temperature profile from the solved optimization algorithm in terms of CSD is further assessed against linear cooling policy to propose the best optimization for the potash alum's seeded batch crystallization process.

## METHODOLOGY

### Mathematical Modelling

A mathematical model was developed in Matlab for one-dimensional and size-dependent potash alum in a water system by using PBE, as shown in Eq. (1), to represent the real process. The assumptions for the process were one-dimensional size-dependent growth, the seed being added to the solution to start the crystallization process, the solution being well-mixed in a batch-jacketed crystallizer, and secondary nucleation, crystal growth, and dissolution were the crystallization phenomena considered. The partial differential equation on the left side represents the population density of  $n$  concerning time,  $t$ , and the growth of crystals relating to particle size,  $L$ , respectively. The birth of nuclei versus time,  $B_{nuc}$ , was shown on the right-hand side of the equation, while the agglomeration and breakage phenomena were not considered.

$$\frac{\partial n(L, t)}{\partial t} + \frac{\partial n(L, t)G(L, C, T)}{\partial L} = B_{nuc} \quad (1)$$

This PBE was then solved numerically using the method of classes shown in Eqs. (2)– (4) by transforming the equation into ordinary differential equations (ODEs) using the 'ode15s' solver in Matlab. For the case of dissolution where relative supersaturation,  $S < 0$ , the growth term,  $G_x$ , was replaced by the dissolution term,  $D_x$ .

$$\frac{dN_1}{dt} + \frac{G_{x1}}{2\Delta Cl_2} N_2 + \frac{G_{x1} - G_{x0}}{2\Delta Cl_1} N_1 = B_{nuc} \quad (2)$$

$$\frac{dN_i}{dt} + \frac{G_{xi}}{2\Delta Cl_{i+1}} N_{i+1} + \frac{G_{xi} - G_{xi-1}}{2\Delta Cl_i} N_i + \frac{G_{xi-1}}{2\Delta Cl_{i-1}} N_{i-1} = 0 \quad (3)$$

$$\frac{dN_n}{dt} + \frac{G_x}{2\Delta Cl} N_n + \frac{G_x}{2\Delta Cl} N_{n-1} = 0 \quad (4)$$

The kinetic models of  $B_{nuc}$ ,  $G_x$ , and  $D_x$  are shown in Eqs. (5)– (7) where all models were dependent on relative supersaturation,  $S$ .  $S = (C - C_{sat})/C_{sat}$  was applied to the model equations. Then, the mathematical model was solved using the parameters and initial conditions shown in Table 1.

$$B_{nuc} = k_b S^b V \quad (5)$$

$$G_{xi} = k_g S^g (1 + \alpha_g L_{xi})^{\beta_g} \quad (6)$$

$$D_{xi} = k_d S^d (1 + \alpha_d L_{xi})^{\beta_d} \quad (7)$$

**Table 1.** Model parameters and initial conditions of the process

Parameters	
$C_{sat}$	$C_{sat} = 3.63 + 0.0243T + 0.00358T^2$
$B_{nuc}$	$B_{nuc} = 0.0380(S)^{3.4174} 1^{-5}$
$G_x$	$G_{xi} = 8.5708(S)^1 (1 + 0.005(L_{xi}))^{1.5777}$
$D_x$	$D_{xi} = 1.28(S)^{0.98} (1 + 0.02(L_{xi}))^{0.86}$
$n_{feed}$	90
$T_{feed}$	40.0
$T_{final}$	17.0
$C_0$	0.104
$\rho_c$	$1.75 \times 10^3$
$k_v$	0.62

The CSD,  $f_n$  can be calculated based on Eq. (8) since the method of classes (MOC) was used to solve PBE, where the size coordinate was discretized into discrete size bins.

$$f_n(L_{xi}) = \frac{1}{2} \left( \frac{N_i + N_{i+1}}{\Delta Cl} \right) \quad (8)$$

### Optimization Strategies

The seeded batch crystallization process was simulated using potash alum in water for four chosen optimization algorithms to achieve the best CSD profile. The optimization algorithms with objective functions of maximizing mean crystal size (I), minimizing CV (II), and minimizing nucleus-grown crystals (III) were selected from the literature because these are frequently used in the literature for achieving optimal cooling profiles. The dissolution algorithm of maximizing CSD (IV) has been considered to be of recent interest. These optimization algorithms were integrated, especially in the equations of the algorithm with the method of classes for consistent interpretation of CSD throughout the simulations, and thus, were shown in Table 2.

To ensure a suitable temperature trajectory, different constraints included minimum and maximum temperature, minimum and maximum temperature ramp rates, the final concentration of solute limited by the maximum final concentration set for the process, and decision variables containing slopes of  $dT/dt$ . These optimization algorithms are solved in Matlab using sequential quadratic programming (SQP) under the 'fmincon' function.

**Table 2.** Summary of selected optimization algorithm from the literature

	<b>Objective Functions</b>	<b>References</b>
I	Max. mean crystal size $\max L_{xi}$ w.r.t. $T_{min} \leq T \leq T_{max}$ $R_{min} \leq dT/dt \leq R_{max}$ $C_{final} \leq C_{final,max}$	Sanzida and Nagy (2019)
II	Min. CV $\min \left[ \left( \left( \frac{N_i}{\Delta Cl_i} \right) + \left( \frac{N_{i+1}}{\Delta Cl_{i+1}} \right) / 2 \right) - 1 \right]^{1/2}$ w.r.t. $T_{min} \leq T \leq T_{max}$ $R_{min} \leq \frac{dT}{dt} \leq R_{max}$ $C_{final} \leq C_{final,max}$	Ashraf and Rao (2022)
III	Min. Nucleus-grown crystals $\min f_n (250\mu m)$ w.r.t. $T_{min} \leq T \leq T_{max}$ $R_{min} \leq dT/dt \leq R_{max}$ $C_{final} \leq C_{final,max}$	Seki and Su (2015)
IV	Max. CSD $\min \sum_{i=1}^N (f_n(L_{xi}) - f_n^{target}(L_{xi}))^2$ w.r.t. $\theta_{T,min} \leq \theta_T \leq \theta_{T,max}$ $0 \leq t_f \leq t_{f,max}$ $C_{final} \leq C_{final,max}$	Nagy <i>et al.</i> (2019)

## RESULTS AND DISCUSSION

Figures 1 to 4 show the seeded batch crystallization process simulation results for the potash alum case study in an open-loop strategy. Figure 1 shows the temperature profiles for linear, and optimizations labeled I, II, III, and IV. The linear cooling profile serves as the reference profile for analyzing all the optimizations for the potash alum crystallization process, whereby the temperature of its solution was reduced from 40 to 17 °C linearly. The temperature profile of optimization I, which is the maximization of mean crystal length obtained by solving the optimization algorithm in Table 2, follows the cubic cooling profile and descends accordingly from 40 to 17 °C. The potash alum solution for optimization II, which minimizes CV, has a smaller cubic curve of temperature

(faster temperature drop) with a similar temperature reduction to optimization I. Optimization III, which minimizes nucleus-grown crystals, also has a similar decrease in temperature but with a larger cubic curve (slower temperature drop) compared to optimizations I and II. Lastly, optimization IV, which maximizes CSD, has a temperature profile that is different from others. It linearly decreased from 40 to 21.8 °C, then increased linearly to 30 °C, and linearly decreased until 17 °C. These temperature profiles all result from the solved optimization algorithms in Table 2. Different temperature profiles are obtained for each objective function as different objectives have different pre-set values of constraints. Different temperature drop for cubic cooling policy was applied for the optimization I to III as this cubic strategy is well established for maximizing CSD,

reducing CV, and suppressing secondary nucleation in literature (Ashraf and Rao, 2022; Hojjati and Rohani, 2005; Nagy *et al.*, 2019). Then, these pre-set constraints generate a specific temperature profile for the selected process, as shown in Figure 1 (Hemalatha *et al.*, 2018).

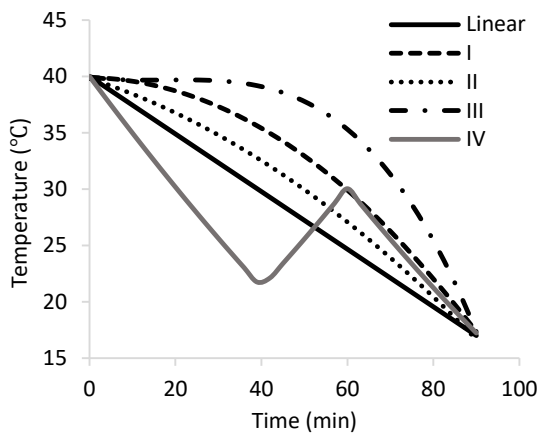


**Fig. 1:** Temperature profiles of all strategies

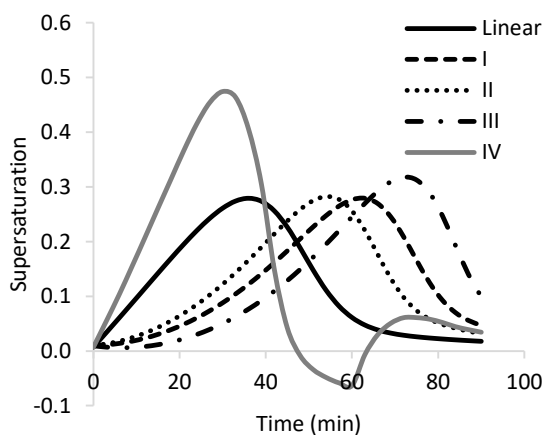


**Fig. 2:** Supersaturation profiles of all strategies

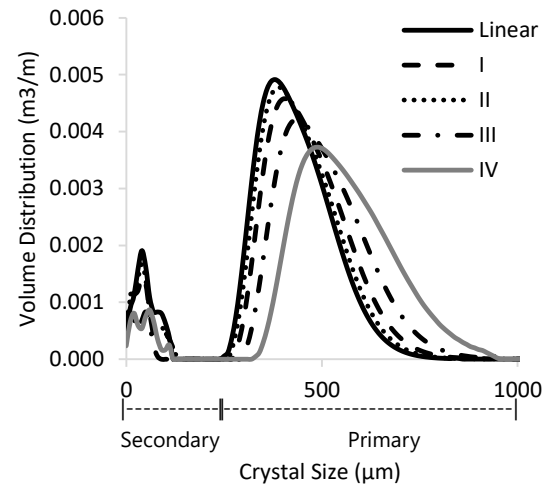
Next, Figure 2 displays the results of supersaturation profiles for each potash alum crystallization process optimization. Compared to the supersaturation profile of the linear cooling curve, which peaks at 36 minutes of operation, optimization I has a peak of supersaturation at 63 minutes of operation despite having the same

supersaturation value at 0.279. This supersaturation profile corresponds to the drop in temperature profile, whether fast or slow, as supersaturation is a temperature-dependent equation (Lee *et al.*, 2019). This equation of  $C_{sat}$  shows this in Table 1, which involves the calculation of relative supersaturation,  $S$ . Since the temperature profile generated in optimization I was dropped slowly following the cubic cooling trend, the peak of supersaturation was shifted to the latter operation time. For optimization II, the supersaturation profile has a peak of 0.282 at an operation time of 54 minutes. Since it has a faster rate of temperature drop compared to optimization I earlier peak of supersaturation is expected. Optimization III, which has the slowest decrement of temperature amongst others, has a peak of supersaturation later than others at 72 minutes of operation and a value of 0.318. The high value of supersaturation's peak, compared to optimization I and II, is due to the steepest drop in temperature to reach 17 °C after 40 minutes of slow decrement in temperature. Lastly, optimization IV, which has different stages of decrement and increment of temperature, contributed to three different peaks of supersaturation. The first stage of decreased temperature from 40 to 21.8 °C has the highest peak compared to other optimizations at 30 minutes of operations with a value of 0.474. This is because its temperature slope at this stage is the steepest compared to others. In the second stage, where the temperature is increased to 30 °C, the supersaturation peak falls inside the negative range at -0.063. This negative supersaturation value represents the dissolution stage, where the growth of crystals is reversed. Finally, the last decreased temperature stage has a small peak of supersaturation at 75 minutes of operation

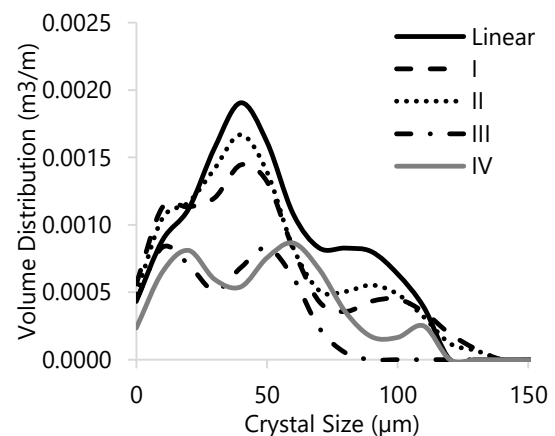
with a value of 0.061. Optimization IV supersaturation profile is the only one with a negative range of supersaturation because its temperature profile had a heating cycle from 40 to 60 minutes of operation, unlike other profiles. This heating cycle generates negative supersaturation, as shown in Figure 2. All these supersaturation trends displayed by all optimizations indirectly translate to the nucleation, growth, and dissolution rates of the crystals, which facilitate the formation of distributed crystals. Supersaturation has a proven relationship with each respective rate, where a high peak of positive supersaturation signifies high nucleation and crystal growth rates. In contrast, a negative peak means a high dissolution rate (Adnan *et al.*, 2019). Based on the results in Figures 1 and 2, the impact of the supersaturation-temperature relationship is consistent with the fundamentals of the crystallization process, which indicates that a fast temperature drop will have a high supersaturation level that contributes to high growth and nucleation rate (Hojjati and Rohani, 2005; Lee *et al.*, 2019).

Figure 3 shows the final CSD of each optimization against the linear cooling profile resulting from the supersaturation value of each profile. In contrast, Figure 4 shows the close-up of secondary peaks for all strategies. Each optimization strategy has two peaks of the final CSD: primary and secondary. The existence of a secondary peak despite a primary peak (grown seed crystals) is expected for all cases as the supersaturation-dependent mechanism of nucleation and crystal growth co-exist concurrently in line with the fundamentals of crystallization (Lee *et al.*, 2019; Nagy *et al.*, 2019). The primary peak is the grown seed crystals ranging from 250 to 1000  $\mu\text{m}$ , and the secondary peak represents the nucleus-grown crystals

ranging less than 250  $\mu\text{m}$ . Mean crystal size is the average crystal size in the CSD data, while volume distribution represents the area under the CSD's curve.



**Fig. 3:** Final CSD of all strategies



**Fig. 4:** Secondary peaks of all strategies

For optimization I, the primary peak is larger in terms of mean crystal size, and the secondary peak is smaller in volume compared to the CSD of linear strategy. This indicates the supersaturation profile of optimization strategy I is slowly increasing from the beginning of the process due to a slower temperature decrement, resulting in better-grown seed distribution and suppression of nucleated crystals compared to linear strategy. Optimization II, it has

almost similar primary and secondary peaks compared to the linear strategy. This is because it has a temperature profile closer to a linear cooling profile. Meanwhile, optimization III has a larger CSD and smaller secondary peak volume than linear and optimizations I and II. This is consistent with the trends of its temperature and supersaturation profiles against those three. Optimization IV, however, has the largest size of primary peak but has a similar volume of secondary peak with optimization III. This may be due to its high supersaturation profile, which induced high nucleation and crystal growth rates. The dissolution stage (negative supersaturation) does not have enough room to reduce fine crystals formed by the previous high nucleation rate, thus left with a similar number of fine crystals with optimization III.

**Table 3.** CSD data for all strategies

Strategy	Mean Crystal Size ( $\mu\text{m}$ )		Volume Distribution ( $\text{m}^3/\text{m}$ )	
	Seed	Nucleated	Seed	Nucleated
<b>Linear</b>	380	40	0.00491	0.00191
<b>I</b>	405	40	0.00457	0.00144
<b>II</b>	390	40	0.00478	0.00166
<b>III</b>	440	30	0.00421	0.00071
<b>IV</b>	490	40	0.00373	0.00071

Table 3 summarizes the detailed results of potash alum simulation for each optimization strategy. It is observed that optimization IV has the lowest height and volume distribution in terms of its primary peak at  $0.00373 \text{ m}^3/\text{m}$ . This is because of the dominant size-dependent growth of the crystals, where the crystals will grow more dispersed based on their growth rate (Ashraf and Rao, 2022; Szilagyi and Nagy, 2019). Also, it has the largest mean crystal size of the primary peak at a mean crystal size of  $490 \mu\text{m}$ , which

contributed to the ample amount of time for the seed crystals to grow during its two high supersaturation stages.

Optimizations III and IV have the least and similar volume distribution but differ in mean crystal size, whereas optimization IV has larger crystals than optimization III. As mentioned earlier, the dissolution stage does not offer enough time for the fine crystals generated from the previous high nucleation rate to dissolve completely, thus producing the same number of fine crystals. The different area values under the peak (volume distribution) and CSD for the primary peak of all optimizations are anticipated as these values are highly dependent on both nucleation and crystal growth rates. The supersaturation level of each respective optimization case influences these rates. The same goes for the data for the secondary peak. The data on mean crystal size for the secondary peak may be similar, but the respective data on volume distribution prove otherwise. Thus, from these results, optimization IV provides the best performance in achieving large sizes of grown seed crystals and minimum fines. Also, these results show that different optimization algorithms with different sets of constraints generate different temperature profiles, which result in different optimized final CSD. Therefore, the best optimization algorithm for the selected production target must be carefully chosen.

## CONCLUSIONS

This paper analyses four optimization algorithms for seeded batch potash alum crystallization case study against linear cooling strategy via simulation in Matlab. The optimization algorithms consist of maximizing mean crystal size (I), minimizing

CV (II), minimizing fines (III), and maximizing CSD (IV). From the analysis, optimization IV has the best performance where its final CSD is the largest (490  $\mu\text{m}$ ) in contrast with linear strategy (380  $\mu\text{m}$ ) and has the minimum number of fine crystals at 0.00071  $\text{m}^3/\text{m}$  against 0.00191  $\text{m}^3/\text{m}$  of linear strategy. The dissolution strategy in optimization IV has contributed to minimum fine crystals and larger mean crystal size of grown seed crystals for the potash alum crystallization process. Therefore, the optimal cooling strategy, which has large-grown seed crystals and the least fines, was established for the studied system of potash alum using the dissolution strategy. Future research should be directed at optimizing this dissolution cooling strategy by implementing closed-loop control.

#### ACKNOWLEDGEMENT

Universiti Malaysia Pahang Al-Sultan Abdullah (UMPSA) has provided financial aid for this research through the Doctorate Research Scheme (DRS).

#### NOMENCLATURE

$B_{nuc}$	: birth of nuclei rate [ $\text{cm}^{-3} \text{min}^{-1}$ ]	$f_n$	: crystal size distribution (CSD)
$b$	: nucleation order	$G$	: growth rate [ $\mu\text{m s}^{-1}$ ]
$C$	: solute concentration [g solute g solvent $^{-1}$ ]	$G_x$	: growth rate in length direction [ $\mu\text{m s}^{-1}$ ]
$C_0$	: solute concentration at $t=0$ [g solute g solvent $^{-1}$ ]	$g$	: growth order
$C_{sat}$	: saturation concentration [g solute g solvent $^{-1}$ ]	$j$	: slopes of $dT/dt$
$C_{final}$	: final solute concentration at the end of batch [g solute g solvent $^{-1}$ ]	$k_b$	: kinetic coefficient for nucleation [# particles $\text{cm}^{-3} \text{min}^{-1}$ ]
$D_x$	: death/ dissolution rate [ $\mu\text{m s}^{-1}$ ]	$k_d$	: kinetic coefficient for dissolution [# particles $\text{cm}^{-3} \text{min}^{-1}$ ]
$d$	: dissolution order	$k_g$	: kinetic coefficient for growth [# particles $\text{cm}^{-3} \text{min}^{-1}$ ]
$f$	relative shape function of crystals	$k_v$	: crystal shape factor
		$L$	: particle size [ $\mu\text{m}$ ]
		$L_x$	: length of crystal particles [ $\mu\text{m}$ ]
		$n$	: population density
		$n_{feed}$	: population density of feed [ $\mu\text{m}$ ]
		$N$	: number of bins
		$N_i$	: Number of crystals per class $i$ [# particles $\text{cm}^{-3}$ ]
		$R$	: temperature ramp [ $^{\circ}\text{C}$ ]
		$S$	: relative supersaturation
		$S^b$	: supersaturation for nucleation
		$S^d$	: supersaturation for dissolution
		$S^g$	: supersaturation for growth
		$T$	: temperature [ $^{\circ}\text{C}$ ]
		$t$	: crystallization time [min]
		$t_f$	: batch duration [min]
		$T_{feed}$	: feed temperature [ $^{\circ}\text{C}$ ]
		$T_{final}$	: final batch temperature [ $^{\circ}\text{C}$ ]
		$V$	: mean crystal volume [ $\text{cm}^3$ ]
		$\rho_c$	: density of crystals [ $\text{kg m}^{-3}$ ]
		$\alpha_d$	: dissolution parameter
		$\alpha_g$	: growth parameter
		$\theta_T$	: decision variables for temperature
		$\beta_d$	: dissolution parameter
		$\beta_g$	: growth parameter
		$\Delta Cl$	: size of class [ $\mu\text{m}$ ]

---

**REFERENCES**

- Aamir, E., 2010. "Population Balance Model-Based Optimal Control of Batch Crystallisation Processes for Systematic Crystal Size Distribution Design." PhD thesis. Loughborough University, Leicestershire, England.
- Adnan, S.Z., Saleh, S., and Samad, N.A.F.A., 2019. "Evaluation of controlled cooling for seeded batch crystallization incorporating dissolution," in: AIP Conference Proceedings. AIP Publishing, pp. 020042-1-020042-8.
- Adnan, S.Z., and Samad, N.A.F.A., 2022. "Effects of nucleation and crystal growth rates on crystal size distribution for seeded batch potash alum crystallization process." *ASEAN J. Chem. Eng.* 22, 258-273.
- Agrawal, S.G., and Paterson, A.H.J., 2015. "Secondary nucleation: mechanisms and models." *Chem. Eng. Commun.* 202, 698-706.
- Ashraf, A.B., and Rao, C.S., 2022. "Multiobjective temperature trajectory optimization for unseeded batch cooling crystallization of aspirin." *Comput. Chem. Eng.* 160, 107704.
- Hemalatha, K., Nagveni, P., Kumar, P.N., and Rani, K.Y., 2018. "Multiobjective optimization and experimental validation for batch cooling crystallization of citric acid anhydrate." *Comput. Chem. Eng.* 112, 292-303.
- Hojjati, H., and Rohani, S., 2005. "Cooling and seeding effect on supersaturation and final crystal size distribution (CSD) of ammonium sulphate in a batch crystallizer." *Chem. Eng. Process. Process Intensif.* 44, 949-957.
- Lee, A.Y., Erdemir, D., and Myerson, A.S., 2019. "Crystals and Crystal Growth," in: Handbook of Industrial Crystallization. Cambridge University Press, pp. 32-75.
- Nagy, Z.K., Fujiwara, M., and Braatz, R.D., 2019. "Monitoring and Advanced Control of Crystallization Processes," in: Handbook of Industrial Crystallization. Cambridge University Press, pp. 313-345.
- Samad, N.A.F.A., Singh, R., Sin, G., Gernaey, K. V., and Gani, R., 2010. "Control of process operations and monitoring of product qualities through generic model-based in batch cooling crystallization." *Comput. Aided Chem. Eng.* 28, 613-618.
- Sanzida, N., and Nagy, Z.K., 2019. "Strategic evaluation of different direct nucleation control approaches for controlling batch cooling crystallisation via simulation and experimental case studies." *Comput. Chem. Eng.* 130, 106559.
- Seki, H., and Su, Y., 2015. "Robust optimal temperature swing operations for size control of seeded batch cooling crystallization." *Chem. Eng. Sci.* 133, 16-23.
- Szilágyi, B., 2022. "External fine particle removal for crystallization processes: Introduction and systematic comparison with the temperature cycling-based fines removal." *Chem. Eng. Process. Process Intensif.* 179, 109074.
- Szilagy, B., and Nagy, Z.K., 2019. "Model-based analysis and quality-by-design framework for high aspect ratio crystals in crystallizer-wet mill systems using GPU acceleration enabled optimization." *Comput. Chem. Eng.* 126, 421-433.
- Trampuž, M., Teslić, D., and Likozar, B., 2021. "Crystal-size distribution-based dynamic process modelling,
-

optimization, and scaling for seeded batch cooling crystallization of Active Pharmaceutical Ingredients (API)."  
*Chem. Eng. Res. Des.* 165, 254–269.

Walla, B., Bischoff, D., Corona Viramontes, I., Montes Figueredo, S., and Weuster-Botz, D., 2023. "Recent advances in the monitoring of protein crystallization processes in downstream processing."  
*Crystals* 13, 773.

Zhang, D., Liu, L., Xu, S., Du, S., Dong, W., and Gong, J., 2018. "Optimization of cooling strategy and seeding by FBRM analysis of batch crystallization." *J. Cryst. Growth* 486, 1–9.

Zheng, Y., Wang, X., and Wu, Z., 2022. "Machine learning modeling and predictive control of the batch crystallization process." *Ind. Eng. Chem. Res.* 61, 5578–5592.

Zong, S., Zhou, G., Li, M., and Wang, X., 2023. "Deep learning-based on-line image analysis for continuous industrial crystallization processes." *Particuology* 74, 173–183.

---